https://doi.org/10.5194/egusphere-2023-2009
Preprint. Discussion started: 13 October 2023

Reaction of SO_3 with H_2SO_4 and Its Implication for Aerosol Particle Formation in the Gas Phase and at the Air-Water Interface

Rui Wang [a], Yang Cheng [a,‡], Yue Hu [a,‡], Shasha Chen [a], Xiaokai Guo [c], Fengmin Song [a], Hao Li [b,*], Tianlei Zhang [a,*]

[a] *Shaanxi Key Laboratory of Catalysis, School of Chemical & Environment Science, Shaanxi University of Technology, Hanzhong, Shaanxi 723001, P. R. China*

[b] *State Key Joint Laboratory of Environment Simulation and Pollution Control, Research Center for Eco-environmental Sciences, Chinese Academy of Sciences, Beijing, 100085, China*

[c] *Department of Applied Chemistry, Yuncheng University, Yuncheng, Shanxi 044000, China*

Abstract

The reactions between SO_3 and atmospheric acids are indispensable in improving the formation of aerosol particle. However, relative to those of SO_3 with organic acids, the reaction of SO_3 with inorganic acids has not received much attention. Here, we explore the atmospheric reaction between SO_3 and H_2SO_4, a typical inorganic acid, in the gas phase and at the air-water interface by using quantum chemical (QC) calculations and Born-Oppenheimer molecular dynamics simulations. We also report the effect of $H_2S_2O_7$, the product of the reaction between SO_3 and H_2SO_4, on new particle formation (NPF) in various environments by using the Atmospheric Cluster Dynamics Code kinetic model and the QC calculation. The present findings show that the gas phase reactions of SO_3 + H_2SO_4 without and with water molecule are both low energy barrier processes. With the involvement of interfacial water molecules, H_2O-induced the formation of $S_2O_7^{2-}\cdots H_3O^+$ ion pair, HSO_4^- mediated the formation of $HSO_4^-\cdots H_3O^+$ ion pair and the deprotonation of $H_2S_2O_7$ were observed and proceeded on the picosecond time-scale. The present findings suggest the potential contribution of SO_3-H_2SO_4 reaction to NPF and aerosol particle growth as the facts that *i*) $H_2S_2O_7$ can directly participate in H_2SO_4-NH_3-based cluster formation and can facilitate the fastest possible rate of NPF from H_2SO_4-NH_3-based clusters by about a factor of 6.92 orders of magnitude at 278.15 K; and *ii*) the formed interfacial $S_2O_7^{2-}$ can attract candidate species from the gas phase to the water surface, and thus, accelerate particle growth.

* Corresponding authors. Tel: +86-0916-2641083, Fax: +86-0916-2641083.

E-mail: ztianlei88@l63.com (T. L Zhang) ; haol@rcees.ac.cn (H. Li)

‡ Yang Cheng and Yue Hu contributed equally to this work.

https://doi.org/10.5194/egusphere-2023-2009
Preprint. Discussion started: 13 October 2023

1. Introduction

Sulfur trioxide (SO_3) is a major air pollutant (Zhuang and Pavlish, 2012; Chen and Bhattacharya, 2013; Cao et al., 2010; Kikuchi, 2001; Mitsui et al., 2011) and can be considered as the most important oxidation product of SO_2 (Starik et al., 2004). As an active atmospheric species, SO_3 can lead to the formations of acid rain and atmospheric aerosol (Sipilä et al., 2010; Mackenzie et al., 2015; England et al., 2000; Li et al., 2016; Renard et al., 2004) and thus plays a well-documented role in regional climate and human health (Zhang et al., 2012; Pöschl, 2005; Zhang et al., 2015; Pöschl and Shiraiwa, 2015; Haywood and Boucher, 2000; Lohmann and Feichter, 2005). In the atmosphere, the hydrolysis of SO_3 to product H_2SO_4 (SA) is the most major loss route of SO_3 (Morokuma and Muguruma, 1994; Akhmatskaya et al., 1997; Larson et al., 2000; Hazra and Sinha, 2011; Long et al., 2013a; Torrent-Sucarrat et al., 2012; Ma et al., 2020). As a complement to the loss of SO_3, ammonolysis reaction of SO_3 in polluted areas of NH_3 can form H_2NSO_3H, which not only can be competitive with the formation of SA from the hydrolysis reaction of SO_3, but also can enhance the formation rates of sulfuric acid (SA)-dimethylamine ($NH(CH_3)_2$, DMA) clusters by about 2 times. Similarity, the reactions of SO_3 with CH_3OH and organic acids (such as HCOOH) were reported (Liu et al., 2019; Hazra and Sinha, 2011; Long et al., 2012; Mackenzie et al., 2015; Huff et al., 2017; Smith et al., 2017; Li et al., 2018a), and both processes can provide a mechanism for incorporating organic matter into aerosol particles. However, the reaction mechanism between SO_3 and inorganic species are still unclear.

As a typical inorganic acid, SA can act as an important role in the new particle formation (Weber et al., 1995; Weber et al., 1996; Weber et al., 2001; Sihto et al., 2006; Riipinen et al., 2007; Sipilä et al., 2010; Zhang et al., 2012) and acid rain (Calvert et al., 1985; Finlayson-Pitts and Pitts Jr, 1986; Wayne, 2000). The source of gas-phase SA is mainly produced by the gas-phase hydrolysis reaction of SO_3. For the direct reaction between SO_3 and H_2O, it takes place hardly in the atmosphere due to high energy barrier (Chen and Plummer, 1985; Hofmann and Schleyer, 1994; Morokuma and Muguruma, 1994; Steudel, 1995). However the addition of a second water molecule (Morokuma and Muguruma, 1994; Larson et al., 2000; Loerting and Liedl, 2000), the hydroperoxyl radical (Gonzalez et al., 2010), formic acid (Hazra and Sinha, 2011; Long et al., 2012) , sulfuric acid (Torrent-Sucarrat et al., 2012), nitric acid (Long et al., 2013a), oxalic acid (Lv et al., 2019) and

https://doi.org/10.5194/egusphere-2023-2009
Preprint. Discussion started: 13 October 2023

ammonia (Bandyopadhyay et al., 2017) have been reported to catalyze the formation of SA from the hydrolysis reaction of SO_3 as they can promote atmospheric proton transfer reactions. Similarity, as SA can give out protons more readily than H_2O, which in turn is more conducive to the proton transfer, thus we predict that the addition reaction involving the proton transfer between SO_3 and SA is much easier under atmospheric conditions that between SO_3 and H_2O. However, this gas-phase reaction has not been investigated as far as we know. Meanwhile, in many gas phase reactions, single water molecule can play a catalyst role by increasing the stability of pre-reactive complexes and reducing the activation energy of transition states (Kanno et al., 2006; Stone and Rowley, 2005; Chen et al., 2014; Viegas and Varandas, 2012, 2016). For example, single water molecule in the $H_2O\cdots HO_2 + SO_3$ reaction can catalyze the formation of HSO_5 (Gonzalez et al., 2010). Thus, it is equally important to study the SO_3 + SA reaction without and with H_2O. In addition to the gas phase reactions, many new atmospheric processes and new reaction pathways have been observed at the air-water interface (Zhong et al., 2017; Kumar et al., 2017; Kumar et al., 2018; Zhu et al., 2016; Li et al., 2016; Zhu et al., 2017). Such as, the organic acids reacting with SO_3 can form the ion pair of carboxylic sulfuric anhydride and hydronium at the air-water interface (Zhong et al., 2019). This mechanism is different from the gas phase reaction in which the organic acid either serves as a catalyst for the hydrolysis of SO_3 or acts as a reactant reacting with SO_3 directly. So, water droplets may play important roles in atmospheric behaviors between SO_3 and SA. Thus, it is also important to study the interfacial mechanism between SO_3 and SA, and to compare its difference with the corresponding gas-phase reaction.

Previous experimental studies (Otto and Steudel, 2001; Abedi and Farrokhpour, 2013) found that disulfuric acid ($H_2S_2O_7$, DSA) is the product of the reaction between SO_3 and SA. From the perspective of structure, DSA possesses two HO functional groups. Both HO groups can act as hydrogen donors and acceptors to interact with atmospheric particle precursors. It has been shown that the products of SO_3 with some important atmospheric species have been identified in promoting NPF process. For example, the products of NH_2SO_3H, $HOOCOOSO_3H$, CH_3OSO_3H and $HOCCOOSO_3H$ from the reactions of SO_3 with NH_3 (Li et al., 2018a), $H_2C_2O_4$ (Yang et al., 2021), CH_3OH (Liu et al., 2019) and HOOCCHO (Rong et al., 2020) all have a catalytic effect on the formation of new particles in aerosols. However, whether DSA produced by the reaction between SO_3 and SA contributes to aerosol formation or not is still unclear. Thus, another main question that

https://doi.org/10.5194/egusphere-2023-2009
Preprint. Discussion started: 13 October 2023

we intend to address here is the role of DSA in atmospheric SA-NH_3 (A) nucleation, which have been recognized as dominant precursors in highly polluted areas, especially in some megacities in Asia.

In this work, using quantum chemical calculations and Master Equation, we first studied the gas-phase reaction between SO_3 and SA to product DSA with H_2O acting as a catalyst. Then, we use the Born-Oppenheimer Molecular Dynamic (BOMD) simulations to evaluate the reaction mechanism of SO_3 with SA at the air-water interface. Finally, we used Atmospheric Clusters Dynamic Code (ACDC) and quantum chemical calculations to investigate atmospheric implications of SO_3-SA reaction to the atmospheric particle formation. Particular attention of this work is focused on the study of *i*) the mechanism difference of the SO_3 + SA reaction in the gas phase and at the air-water interface; *ii*) the fate of DSA in atmospheric NPF and its influence at various environmental conditions.

2. Computational Details

2.1 Quantum Chemical Calculation. For the gas-phase reaction of SO_3 + SA without and with water molecule, the optimized geometries and vibrational frequencies of reactants, pre-reactive complexes, transition states (TSs), post-reactive complexes and products were calculated using M06-2X method (Frisch et al., 1990) with 6-311++G(2*df*,2*pd*) basis set by Gaussian 09 packages (Frisch, 2009). At the same level, the connectivity between the TSs and the suitable pre- and post-reactant complexes was performed by intrinsic reaction coordinate (IRC) calculations. Then, single point energy calculations were calculated at the CCSD(T)-F12/cc-pVDZ-F12 level by using ORCA (Bork et al., 2014; Myllys et al., 2016; Elm and Kristensen, 2017).

A multistep global minimum sampling technique was used to search for the global minima of the $(DSA)_x(SA)_y(A)_z$ ($z \leq x + y \leq 3$) molecular clusters. In the first step, the initial structure of 1000 clusters were autogenerated by the ABCluster program (Zhang and Dolg, 2015, 2016) with the CHARMM force field (MacKerell et al., 1998). Then, these structures were optimized firstly by the semiempirical PM6 method in Mopac 2016 (Stewart, 2016). Next, up to 100 isomers were reoptimized at the M06-2X/6-31+G(*d*,*p*) level. Finally, 10 lowest-lying structures were optimized by the M06-2X/6-311++G(2*df*,2*pd*) level to determine the global minimum. The optimized structures and the formation Gibbs free energy of the stable clusters were summarized in Fig. S9

https://doi.org/10.5194/egusphere-2023-2009
Preprint. Discussion started: 13 October 2023

and Table S8 of the *SI Appendix*, respectively.

2.2 Rate constant calculations. Using the Rice-Ramsperger-Kassel-Marcus based Master Equation (ME/RRKM) model (Miller and Klippenstein, 2006), the kinetics for the SO_3 + SA reaction without and with water molecule were calculated by adopting a Master Equation Solver for Multi Energy-well Reactions (MESMER) code (Glowacki et al., 2012). In the MESMER calculation, the rate coefficients for the bimolecular barrierless association step (from reactants to pre-reactive complexes) were evaluated by the Inverse Laplace Transform (ILT) method (Horváth et al., 2020), meanwhile the unimolecular step was performed by the RRKM theory combined with the asymmetric Eckart model. The ILT method and RRKM theory can be represented in Eq (1) and Eq (2), respectively.

$$k^{\infty}(\beta) = \frac{1}{Q(\beta)} \int_0^{\infty} k(E)\rho(E)\exp(-\beta E)dE \quad (1)$$

$$k(E) = \frac{W(E - E_0)}{h\rho(E)} \quad (2)$$

Where h is denoted as Planck's constant; $\rho(E)$ is denoted as the active density of state of the reactant at energy level E; E_0 is denoted as the reaction threshold energy and $W(E\text{-}E_0)$ is denoted as the sum of the rovibrational states of the transition state (TS) geometry (excluding the degree of freedom related to passing the transition state). The input parameters for electronic geometries, vibrational frequencies, and rotational constants were calculated at the M06-2X/6-311++G(2*df*,2*pd*) level and single-point energy calculations were refined at the CCSD(T)-F12/cc-pVDZ-F12 level for the modeling.

2.3 Born-Oppenheimer Molecular Dynamic (BOMD) Simulation. The CP2K code (Hutter et al., 2014) was used in the BOMD simulations. The Becke-Lee-Yang-Parr (BLYP) functional (Becke, 1988; Lee et al., 1988) was chosen to treat with the exchange and correlation interactions, and the Grimme's dispersion was carried out to account for the weak dispersion interaction (Grimme et al., 2010). The Goedecker-Teter-Hutter (GTH) conservation pseudopotential (Goedecker et al., 1996; Hartwigsen et al., 1998) with the Gaussian DZVP basis set (VandeVondele and Hutter, 2007) and the auxiliary plane wave basis set was applied to correct the system valence electrons and the core electrons, respectively. For the plane wave basis set and Gaussian basis set, the energy cut off (Zhong et al., 2017; Zhong et al., 2018;

https://doi.org/10.5194/egusphere-2023-2009
Preprint. Discussion started: 13 October 2023

Zhong et al., 2019) were set to 280 and 40 Ry, respectively. For each simulation in the gas phase, a 15 × 15 × 15 $Å^3$ supercell with periodic boundary condition was adopted with a time step of 0.5 fs. The air-water interfacial system included 191 water molecules, SO_3 and SA in the BOMD simulation. To avoid periodic interactions between adjacent water droplets, the size of the simulation box (Kumar et al., 2017; Kumar et al., 2018; Ma et al., 2020) was set as 35 × 35 × 35 $Å^3$ with a time step of 1.0 fs. For all the simulations in the gas phase and at the air-water interface, the Nose-Hoover thermostat (Zhong et al., 2017; Zhong et al., 2018; Zhong et al., 2019; Kumar et al., 2017; Kumar et al., 2018; Ma et al., 2020) was selected the NVT ensemble to control the temperature around 300 K.

2.4 Atmospheric Clusters Dynamic Code (ACDC) Model

The Atmospheric Cluster Dynamics Code (ACDC) (McGrath et al., 2012) was used to simulate the cluster formation rates and mechanisms of $(DSA)_x(SA)_y(A)_z$ ($z \leq x + y \leq 3$) clusters at different temperatures and monomer concentrations. The thermodynamic data of quantum chemical calculation at the DLPNO-CCSD(T)/aug-cc-pVTZ//M06-2X/6-311++G (2*df*,2*pd*) level of theory can be used as the input of ACDC. The birth-death equation (Eq. 3) for clusters solves the time development of cluster concentrations by numerical integration using the ode15s solver in MATLAB program (Shampine and Reichelt, 1997).

$$\frac{dc_i}{dt} = \frac{1}{2}\sum_{j<i}\beta_{j,(i-j)}C_jC_{(i-j)} + \sum_j \gamma_{(i+j)\to i}C_{i+j} - \sum_j \beta_{i,j}C_iC_j - \frac{1}{2}\sum_{j<i}\gamma_{i\to j}C_i + Q_i - S_i \qquad (3)$$

Where c_i is the concentration of cluster i; $\beta_{i,j}$ is the collision coefficient between clusters i and j; $\gamma_{(i+j)\to i}$ is the evaporation coefficient of cluster $i+j$ evaporating into clusters i and j, and Q_i is all other source term of cluster i. (See more details of β and γ in *SI Appendix* Part 4). Besides, a constant coagulation sink coefficient 2 × 10^{-2} s^{-1} (corresponding to the median observed in contaminated areas) was used for taking into account external losses (Yao et al., 2018; Zhang et al., 2022; Liu et al., 2021b). The details for the boundary conditions and concentration ranges of SA, A and DSA are presented in the *SI Appendix* Part 5.

3. Results and discussion

3.1 Reactions in the gas phase

The addition reaction involving the proton transfer between SO_3 and SA (Channel DSA)

https://doi.org/10.5194/egusphere-2023-2009
Preprint. Discussion started: 13 October 2023

proceeded through the formation of $SO_3\cdots H_2SO_4$ complex followed by unimolecular transformation through transition state TS_{DSA} to form $H_2S_2O_7$ (Fig. 1(a)). The reactant complex $SO_3\cdots H_2SO_4$ was a double six-membered ring complex with a relative Gibbs free energy of -1.6 kcal·mol^{-1}. After the formation of $SO_3\cdots H_2SO_4$ complex, Channel DSA overcame a Gibbs free energy barrier of 2.3 kcal·mol^{-1}, which was lower by 4.2 kcal·mol^{-1} than that of H_2O-catalyzed hydrolysis of SO_3 (Fig. S1). Rate constant for the SO_3 + SA reaction was calculated at various temperatures (Table 1). Within the temperature range of 280-320 K, the rate constants for the SO_3 + SA reaction were calculated to be 2.57×10^{-12}-5.52×10^{-12} cm^3·molecule^{-1}·s^{-1}, which were larger by 3.43-4.03 times than the corresponding values of H_2O-catalyzed hydrolysis of SO_3. Therefore, it can be said that the direct reaction between SO_3 and SA is more favorable over H_2O-catalyzed hydrolysis of SO_3 energetically and kinetically.

As the probability of simultaneous collision (Pérez-Ríos et al., 2014; Elm et al., 2013) of three molecules of SO_3, SA and H_2O is quite low under realistic conditions, the SO_3 + SA reaction with H_2O (Channel DSA_WM) can be considered as a sequential bimolecular process. In other words, Channel DSA_WM occurs via the collision between SO_3 (or SA) and H_2O to form dimer ($SO_3\cdots H_2O$ and $H_2SO_4\cdots H_2O$) first, and then the dimer encounters with the third reactant SA or SO_3. The computed Gibbs free energies of dimer complexes $SO_3\cdots H_2O$ and $H_2SO_4\cdots H_2O$ were respectively 0.8 kcal·mol^{-1} and -1.9 kcal·mol^{-1}, which were respectively consistent with the previous values (the range from -0.2 to 0.62 kcal·mol^{-1} for $SO_3\cdots H_2O$ complex (Bandyopadhyay et al., 2017; Long et al., 2012) and the range from -1.82 to -2.63 kcal·mol^{-1} for $H_2SO_4\cdots H_2O$ complex (Long et al., 2013b; Tan et al., 2018)). The Gibbs free energy of $H_2SO_4\cdots H_2O$ was lower by 2.7 kcal·mol^{-1} than that of $SO_3\cdots H_2O$, thus leading to that the equilibrium constant of the former complex is larger by at least one order of magnitude than that of the latter one in Table S2. Additionally, the larger equilibrium constant of $H_2SO_4\cdots H_2O$ complex leads to its higher concentration in the atmosphere. For example, when the concentrations of SO_3 (Yao et al., 2020), H_2SO_4 (Liu et al., 2015) and H_2O (Anglada et al., 2013) were 10^6, 10^8 and 10^{17} molecules·cm^{-3}, respectively, the concentrations of $SO_3\cdots H_2O$ and $H_2SO_4\cdots H_2O$ were 2.41×10^3-2.01×10^4 and 5.01×10^5-3.01×10^8 molecules·cm^{-3} within the temperature range of 280-320 K (see Table S3), respectively. So, we predict that Channel DSA_WM mainly takes place via the collision of $H_2SO_4\cdots H_2O$ with SO_3. In order to check this prediction, the effective rate constants for two bimolecular reactions of $H_2SO_4\cdots H_2O$ + SO_3 and

https://doi.org/10.5194/egusphere-2023-2009
Preprint. Discussion started: 13 October 2023

$SO_3\cdots H_2O + H_2SO_4$ were calculated, and the details were shown in *SI Appendix*, Part 3 and Table 1. As seen in Table 1, the $SO_3\cdots H_2O + H_2SO_4$ reaction can be neglected as its effective rate constant is smaller by 16.7-48.5 times than the corresponding value of the $H_2SO_4\cdots H_2O + SO_3$ reaction. Therefore, we only consider the $H_2SO_4\cdots H_2O + SO_3$ bimolecular reaction in H_2O-catalyzed SO_3 + SA reaction.

The $H_2SO_4\cdots H_2O + SO_3$ reaction occurred in a stepwise process as displayed in Fig. 1(b), which was similar to the favorable routes in the hydrolysis of COS, HCHO and CH_3CHO catalyzed by sulfuric acid (Long et al., 2013b; Li et al., 2018b; Tan et al., 2018). When the $H_2SO_4\cdots H_2O$ complex and SO_3 served as reactants, the reaction was initiated by complex IM_{DSA_WM}' where a van der Waals interaction (S2⋯O4, 2.75 Å) was found between the O4 atom of SA moiety in $H_2SO_4\cdots H_2O$ and the S atom of SO_3. After complex IM_{DSA_WM}', the ring enlargement from IM_{DSA_WM}' to $SO_3\cdots H_2SO_4\cdots H_2O$ complex occurred through transition state TS_{DSA_WM}' with a Gibbs free energy barrier of 1.2 kcal·mol^{-1}. Complex $SO_3\cdots H_2SO_4\cdots H_2O$ was 6.1 kcal·mol^{-1} lower in energy than IM_{DSA_WM}'. In $SO_3\cdots H_2SO_4\cdots H_2O$, SO_3 acted as double donors of hydrogen bond to form a cage-like hydrogen bonding network with $H_2SO_4\cdots H_2O$. Then, starting with $SO_3\cdots H_2SO_4\cdots H_2O$ complex, the $H_2SO_4\cdots H_2O + SO_3$ reaction occurred through transition state TS_{DSA_WM} with a Gibbs free barrier energy of 0.5 kcal·mol^{-1} to form a quasi-planar network complex, $H_2S_2O_7\cdots H_2O$. TS_{DSA_WM} was in the middle of a double proton transfer, where H_2O played as a bridge for proton transfer, along with the simultaneous formation of the O4⋯S2 bond. In order to estimate the catalytic ability of H_2O in the SO_3 + SA reaction, the effective rate constant ($k'_{DSA\_WM\_s}$) of the $H_2SO_4\cdots H_2O + SO_3$ reaction were compared with the rate constant (k_{DSA}) of the SO_3 + SA reaction. As seen in Table 1, under the experimental concentration (Anglada et al., 2013) ([H_2O] = 5.20×10^{16}-2.30×10^{18} molecules·cm^{-3}) within the temperature range of 280-320 K, the calculated $k'_{DSA\_WM\_s}$ was 1.03×10^{-11}-4.60×10^{-12} cm^3·molecule^{-1}·s^{-1}, which was larger by 1.79-1.86 times than that of k_{DSA}. This result shows that H_2O exerts catalytic role in promoting the rate of the SO_3 + SA reaction.

3.2 Reactions at the Air-water interface

The mechanism for the SO_3 + SA reaction at the air-water interface was lacking and thus explored below. Due to the high reactivity of SO_3 and SA at the air-water interface, the product SA^- is formed with extremely short times from both SO_3 (Zhong et al., 2019) and SA (Fig. S2) (on the

https://doi.org/10.5194/egusphere-2023-2009
Preprint. Discussion started: 13 October 2023

order of a few picoseconds) with interfacial water molecules. So, two possible models were mainly considered for SO_3-SA reaction on the water surface: (*i*) gaseous SO_3 colliding with SA^- at the air-water interface and (*ii*) the DSA (the gas-phase product of SO_3 and SA) dissociating on water droplet.

Gaseous SO_3 Colliding with SA^- at the Air-Water Interface. At the water droplet's surface, the interaction between SO_3 and SA^- included two main channels: (*i*) H_2O-induced formation of $S_2O_7^{2-}\cdots H_3O^+$ ion pair (Fig. 2, Fig. S3 and Movie S1) and (*ii*) SA^--mediated formation of $SA^-\cdots H_3O^+$ ion pair (Fig. 3, Fig. S4-S5 and Movie S2-S3). The BOMD simulations for H_2O-induced formation of $S_2O_7^{2-}\cdots H_3O^+$ ion pair was illustrated in Fig. 2, the H1 atom of SA^- ion can combine with a nearby interfacial water molecule at 8.18 ps by hydrogen bond ($d_{(O3\text{-}H1)}$ = 1.17 Å) interaction, thus forming hydrated hydrogen sulfate ion ($SA^-\cdots H_2O$). Then, the H1 atom of SA^- ion was moved to the O3 atom of the interfacial water molecule at 8.28 ps, revealing the formation of $SO_4^{2-}\cdots H_3O^+$ ion pair. Additionally, SO_4^{2-} gradually approached to SO_3 molecule with the shortening of S1-O1 bond. At 9.26 ps, the S1-O1 bond length was 1.84 Å, which was close to the length of S-O1 bond in $S_2O_7^{2-}$ ion (Fig. S7), revealing the formation of $S_2O_7^{2-}\cdots H_3O^+$ ion pair. Both direct (without the involvement of SA^-, Fig. 3(a), Fig. S4 and Movie S2) and indirect (with the involvement of SA^-, Fig. 3(b), Fig. S5 and Movie S3) forming mechanisms were observed in SA^--mediated formation of $SA^-\cdots H_3O^+$ ion pair. The direct SA^--mediated formation of $SA^-\cdots H_3O^+$ ion pair was a loop structure mechanism, which was consistent with gas phase hydrolysis of SO_3 assisted by acidic catalysts of HCOOH, HNO_3, $H_2C_2O_4$ and SA in the previous works (Long et al., 2012; Long et al., 2013a; Torrent-Sucarrat et al., 2012; Lv et al., 2019), and HNO_3-mediated Criegee hydration at the air-water interface. As for the direct formation mechanism of $SA^-\cdots H_3O^+$ ion pair seen in Fig. 3(a) and movie S2, an eight-membered loop complex, $SO_3\cdots H_2O(1)\cdots SA^-$, was found at 1.46 ps with the formations of two hydrogen bonds ($d_{(O3\cdots H2)}$ = 2.13 Å; $d_{(O4\cdots H3)}$ = 2.18 Å) and a van der Waals interaction ($d_{(S1\cdots O1)}$ = 2.14 Å). Subsequently, SO_3 and interfacial $H_2O(1)$ were close to each other. At 1.59 ps, a transition state-like loop structure was observed and proton transfer from interfacial $H_2O(1)$ to another suspended $H_2O(2)$ was found, where the bond lengths of S1-O1, O1-H1 and H1-O2 were 1.94 Å, 1.19 Å and 1.32 Å, respectively. At 1.70 ps, the bond lengths of S-O1 and H1-O2 were reduced to 1.73 Å and 1.01 Å, while the bond length of H1-O2 was extended to 1.61 Å, showing the formation of $SA^-\cdots H_3O^+$ ion pair. During the direct formation route of $SA^-\cdots H_3O^+$ ion pair, SA^- played as a spectator, while interfacial water molecules acted as both a reactant and a

https://doi.org/10.5194/egusphere-2023-2009
Preprint. Discussion started: 13 October 2023

proton acceptor.

As seen in Fig. 3(b) and Movie S3, the indirect forming process of $SA^-\cdots H_3O^+$ ion pair contained two steps: (*i*) SO_3 hydration along with SA formation and (*ii*) SA deprotonation. Specifically, as for step (*i*), at 0.70 ps, a transition state like structure of SO_3 hydration was observed with SO_3, SA^- and an interfacial water molecule involved. Note that at this time the H1 atom in interfacial H_2O molecule migrated to the O2 atom of SA^- ion instead of the surrounding water molecule. At 0.96 ps, the O1-H1 bond of H_2O was broken with the length of 1.56 Å, while the S1-O1 bond was formed with the length of 1.75 Å, demonstrating the completion of hydrolysis reaction of SO_3 and the formation of SA molecule. Then, at 8.08 ps, the H2 proton transfer from SA to the O4 atom of SA^- ion to the O5 atom of the nearby water molecule was occurred, where the O3-H2 and O1-H3 bonds extended to 1.13 Å and 1.22 Å, and the length of O4-H2 and O5-H3 bonds shortened to 1.45 Å and 1.20 Å. Finally, SA deprotonation was completed at 8.23 ps with the formation of $SA^-\cdots H_3O^+$ ion pair. During the whole indirect forming process of $SA^-\cdots H_3O^+$ ion pair, SA^- played as protons donor and acceptor, and water molecules acted as hydration reactants and proton acceptors.

The $H_2S_2O_7$ Dissociating on Water Droplet. In addition to the gaseous SO_3 colliding with SA^- at the air-water interface, DSA, the product of the barrierless reaction between SO_3 and SA, can further quickly react with interfacial water molecule at the air-water interface. As seen in Fig. 4, Fig. S6 and Movie S4, DSA is highly reactive at the air-water interface and can undergo two deprotonations to form $S_2O_7^{2-}$ ion. Specifically, the DSA can firstly form a H-bond with interfacial water molecule at 0.45 ps. After that, the H1 atom of DSA transferred to interfacial water and produced $HS_2O_7^-$ and H_3O^+ ions. The formed $HS_2O_7^-$ ion can survive for ~3 ps on water droplet. At 4.14 ps, the H2 atom of $HS_2O_7^-$ ion moved to O4 atom of nearby interfacial water molecule and produced the formation of $S_2O_7^{2-}\cdots H_3O^+$ ion pair, which was stable at the air-water interface over a simulated time scale of 10 ps. Note that the second deprotonation of DSA indeed needs more time than its first deprotonation as the pK_a1 (pK_a1 = -16.05) of DSA is much smaller than its pK_a2 (pK_a2 = -4.81) (Abedi and Farrokhpour, 2013). In brief, at the air-water interface, both these two routes of the formation of $S_2O_7^{2-}\cdots H_3O^+$ ion pair occur on the picosecond time scale.

3.3 Atmospheric Implications

In the gas-phase, the main sink route of SO_3 is H_2O-assisted hydrolysis of SO_3 (Morokuma

https://doi.org/10.5194/egusphere-2023-2009
Preprint. Discussion started: 13 October 2023

and Muguruma, 1994; Akhmatskaya et al., 1997; Larson et al., 2000; Hazra and Sinha, 2011; Long et al., 2013a; Torrent-Sucarrat et al., 2012; Ma et al., 2020). To study the atmospheric importance of the SO_3 + SA reaction without and with H_2O, the rate ratio (v_{DSA}/v_{SA}) between the SO_3 + SA reaction and H_2O-assisted hydrolysis of SO_3 was compared, which was expressed in Eq. (4).

$$\frac{v_{DSA}}{v_{SA}} = \frac{k_{DSA} \times [SO_3] \times [H_2SO_4] + k_{DSA\_WM\_s} \times K_{eq(H_2SO_4 \cdots H_2O)} \times [SO_3] \times [H_2SO_4] \times [H_2O]}{k_{SA\_WM} \times K_{eq(SO_3 \cdots H_2O)} \times [SO_3] \times [H_2O] \times [H_2O]} \quad (4)$$

In Eq. (4), K_{eq1} and K_{eq2} were the equilibrium constant for the formation of complex $H_2SO_4 \cdots H_2O$ and $SO_3 \cdots H_2O$ shown in Table S2, respectively; k_{DSA}, k_{DSA_WM} and k_{SA_WM} were respectively denoted the bimolecular rate coefficient for the H_2SO_4 + SO_3, $H_2SO_4 \cdots H_2O$ + SO_3 and $SO_3 \cdots H_2O$ + H_2O reactions; [H_2O] and [H_2SO_4] were respectively represented the concentration of H_2O and SA taken from references (Anglada et al., 2013; Liu et al., 2015); The value of v_{DSA}/v_{SA} was listed in Table S6. As seen in Table S6, the hydrolysis reaction of SO_3 + $(H_2O)_2$ is usually the major sink route of SO_3, as the [H_2O] is much larger than that of [H_2SO_4] (10^4-10^8 molecules·cm^3). However, the formation of $H_2S_2O_7$ from the gas phase reaction of SO_3 with SA investigated in the present work could play a role in the chemistry of the Earth's atmosphere.

Through the configuration (shown in Fig. S9) and stability analysis (shown in Fig. S10 and Table S8-S11), DSA was found to promote intermolecular interactions between SA and A to stabilize the corresponding clusters. To figure out how DSA affects the kinetic clustering process, the potential influence of DSA to the SA-A-based particle formation was estimated by calculating the enhancement factor *R* in Eq (5).

$$R = \frac{J_{SA\text{-}A\text{-}DSA}}{J_{SA\text{-}A}} = \frac{J([SA] = x, [A] = y, [DSA] = z)}{J([SA] = x, [A] = y, [DSA] = 0)} \quad (5)$$

where $J_{SA\text{-}A\text{-}DSA}$ and $J_{SA\text{-}A}$ are represented the formation rate of SA-A-DSA and SA-A nucleating system, respectively. *x*, *y* and *z* are the atmospheric concentration of SA, A and DSA. As the values of *R* shown in Table S12-S16, DSA was better enhancer for NPF of SA-A based system, because *R* were all greater than or equal to 1.0 at four different temperatures of 218.15 K, 238.15 K, 258.15 K, 278.15 K and 298.15 K as well as the nucleation precursor concentration range ([SA] = 10^6-10^8 molecules·cm^{-3}; [A] = 10^7-10^{11} molecules·cm^{-3} and the calculated DSA concentrations are [DSA] = 10^1-10^3 molecules·cm^{-3} in Table S7).

Generally, *J* and *R* has been affected by the temperature and the concentrations of nucleating

https://doi.org/10.5194/egusphere-2023-2009
Preprint. Discussion started: 13 October 2023

precursors (Liu et al., 2021a). The *J* of SA-A-DSA-based system in Fig. S11 is negatively dependent on temperature, and it sharply rise with the increase of [DSA] at the normal temperature (298.15 K) and the atmospheric pollution boundary layer (278.15 K). However, Fig. 5(a) showed that *R* rises with the increase of temperature, and the rise trend of *R* is relatively more obvious at 298.15 K and 278.15 K which can be up to 7.19 and 3.82 orders of magnitude at higher [DSA], respectively. This behavior may be because that although both the $J_{SA\text{-}A\text{-}DSA}$ and $J_{SA\text{-}A}$ decrease with the temperature increase, the reduction scale of $J_{SA\text{-}A}$ is much greater than that of $J_{SA\text{-}A\text{-}DSA}$ when the temperature is increased from 218.15 K to 298.15 K. Notedly, the values of *J* at 298.15 K are lower by at least two orders of magnitude than that at 278.15 K at higher [DSA]. So, in the following studies, attention is mainly focused on the atmospheric pollution boundary layer (278.15 K). As illustrated in Fig. 5(b), a remarkable rise of *R* with the increase of [A] has been discovered when [A] was larger than 10^9 molecules·cm^{-3} at 278.15 K. The significantly negative correlation of *R* with [SA] in all ranges of [A] (Fig. 5(b)) has been established due to a competitive relationship between SA and DSA. When [DSA] and [A] were the highest and [SA] was the lowest, the effect of *R* was the strongest, and *R* can reach 6.92 orders of magnitude. This conclusions about the change of *R* with concentrations of precursors could also be applied for the other four temperatures shown in Fig. S11. Hence, it can be forecasted that the participation of DSA in SA-A-based NPF can likely enhance the number concentration of atmospheric particulates significantly in the polluted atmospheric boundary layer (278.15 K) areas with relatively high [DSA] and [A].

Two main cluster formation pathways, the pure SA-A-based cluster (a) and DSA-containing cluster (b), can be observed at 278.15 K (Fig. 6(A)). As seen, the DSA molecule exhibited an ability to directly participate in cluster formation under median concentration precursors of SA and DSA, and high [A], indicating that DSA can be a "participator" in promoting cluster formation. Interestingly, at different temperature, the DSA molecule showed different effect mechanism and contribution in SA-A system. As seen in Fig. 6(B), the cluster growth pathways were dominated by pure SA-A-based cluster formation under the conditions of 218.15 K, 238.15 K and 258.15 K, whereas the DSA-containing cluster formation was dominant at 278.15 K. By the way, the cluster growth pathways were completely dominated by the DSA-containing cluster at 298.15 K, and its contribution for growth flux out of the system reached to 100% (Fig. S13). Meanwhile, the relative contribution of the pure SA-A-based cluster pathway and the DSA-containing cluster pathway to

https://doi.org/10.5194/egusphere-2023-2009
Preprint. Discussion started: 13 October 2023

the growth flux out of the system may also depend on the precursors concentration. Specifically, when the temperature was fixed at 278.15 K, the contribution of DSA-containing pathway was positively correlated with [DSA] in Fig. 6(C). Of particular note, at low DSA concentration ([DSA] = 10^1 molecule·cm^{-3}), DSA do not substantially contribute to the cluster growth and the pathway just involved the pure SA-A-based clusters. While at the median concentration of DSA ([DSA] = 10^2 molecule·cm^{-3}), the contribution of DSA-containing clusters for growth flux out of the system can up to 84%. When [DSA] raised to 10^3 molecule·cm^{-3}, the DSA-containing clusters growth mainly dominates cluster formation in the system, and its contribution for growth flux out of the system increased to 95%. Besides, the contribution of DSA-containing pathway was negatively correlated with [SA] because of the competition relationship between DSA and SA shown in Fig. 6(D). These results suggested that DSA has the ability to act as a potential contributor to SA-A-based NPF in the atmosphere, and the DSA participation pathway can be dominant in heavy sulfur oxide polluted atmospheric boundary layer and in season of late autumn and early winter.

At the air-water interface, important implication of the BOMD simulations is that the reaction between SO_3 and SA at the air-water interface can be accomplished within a few picoseconds, among which the interfacial water molecules play a significant role in promoting the formation of $S_2O_7^{2-}\cdots H_3O^+$ and $SA^-\cdots H_3O^+$ ion pairs. Furthermore, the adsorption capacity of the $S_2O_7^{2-}$, H_3O^+ and SA^- to gasous precursors in the atmosphere was further investigated. Herein, the species of SA, NH_3, and HNO_3 have been regarded as the candidate species. (Kulmala et al., 2004; Kirkby et al., 2011). Our calculated results in Table 2 show that the interactions of $S_2O_7^{2-}\cdots H_2SO_4$, $S_2O_7^{2-}\cdots HNO_3$, $S_2O_7^{2-}\cdots(COOH)_2$, $H_3O^+\cdots NH_3$, $H_3O^+\cdots H_2SO_4$, $SA^-\cdots H_2SO_4$, $SA^-\cdots(COOH)_2$, and $SA^-\cdots HNO_3$ are stronger than those of $H_2SO_4\cdots NH_3$ (major precursor of atmospheric aerosols). These results reveal that interfacial $S_2O_7^{2-}$, SA^- and H_3O^+ can attract candidate species from the gas phase to the water surface, and thus in turn accelerates the growth of particle. Moreover, we evaluated the enhancing potential of $S_2O_7^{2-}$ on SA-A cluster by considering geometrical structure and the formation free energies of the $(SA)_1(A)_1(S_2O_7^{2-})_1$ clusters. As compared with $(SA)_1(A)_1(X)_1$ (X = $HOOCCH_2COOH$, $HOCCOOSO_3H$, CH_3OSO_3H, $HOOCCH_2CH(NH_2)COOH$ and $HOCH_2COOH$) clusters (Zhong et al., 2019; Zhang et al., 2018; Rong et al., 2020; Gao et al., 2023; Liu et al., 2021a; Zhang et al., 2017), the number of hydrogen bonds in $(SA)_1(A)_1(S_2O_7^{2-})_1$ cluster presented in Fig. S8 increased and the ring of the complex was enlarged. It was demonstrated that $S_2O_7^{2-}$ has the

https://doi.org/10.5194/egusphere-2023-2009
Preprint. Discussion started: 13 October 2023

highest potential to stabilize SA-A clusters and promote SA-A nucleation in these clusters due to its acidity and structural factors such as more intermolecular hydrogen bond binding sites. Subsequently, comparing to $(SA)_1(A)_1(X)_1$ clusters (Table 2), the Gibbs formation free energy ΔG of $(SA)_1(A)_1(S_2O_7^{2-})_1$ cluster is lower. Therefore, we predict that $S_2O_7^{2-}$ at the air-water interface has important implication to the aerosol NPF in highly industrial polluted regions with high concentrations of SO_3.

4. Summary and Conclusions

In this work, we employed QC calculations, BOMD simulations and ACDC kinetic model to characterize the SO_3-H_2SO_4 interaction in the gas phase and at the air-water interface and to study the effect of $H_2S_2O_7$ on H_2SO_4-NH_3-based clusters. Results revealed that the energy barrier of the gas phase SO_3 + H_2SO_4 reaction without and with H_2O is less than 2.3 kcal·mol^{-1}. Rate constants indicated that though the SO_3 + H_2SO_4 reaction cannot compete with H_2O-assisted hydrolysis of SO_3 within the temperature range of 280-320 K, its rate constant was close to the upper limits for bimolecular reactions and H_2O exerts obvious catalytic role in promoting the reaction rate. Moreover, ACDC kinetic simulations showed that DSA has unexpected facilitate effects on the NPF process and can enhance the rate of NPF from SA-A by about 6.92 orders of magnitude in polluted atmospheric boundary layer. Of particular note, DSA can directly participate in the SA-A-based cluster formation pathway with its contribution up to 93% in regions with atmospheric pollution boundary layer of high concentrations of SO_3, especially in late autumn and early winter.

At the air-water interface, H_2O-induced the formation of $S_2O_7^{2-}\cdots H_3O^+$ ion pair, SA^- mediated the formation of $SA^-\cdots H_3O^+$ ion pair and the deprotonation of $H_2S_2O_7$ were observed，both of which can occur within a few picoseconds. The formed interfacial $S_2O_7^{2-}$, SA^- and H_3O^+ can attract candidate species (such as H_2SO_4, NH_3, and HNO_3) for particle formation from the gas phase to the water surface, and thus accelerates the growth of particle. Moreover, potential of X (X = $S_2O_7^{2-}$, $HOOCCH_2COOH$, $HOCCOOSO_3H$, CH_3OSO_3H, $HOOCCH_2CH(NH_2)COOH$ and $HOCH_2COOH$) in ternary SA-A-X cluster formation indicated that $S_2O_7^{2-}$ has the highest potential to stabilize SA-A clusters and promote SA-A nucleation among X.

The present work will expand our understanding of new pathway for the loss of SO_3 in acidic polluted areas. Moreover, this work will also help to reveal some missing sources of metropolis

https://doi.org/10.5194/egusphere-2023-2009
Preprint. Discussion started: 13 October 2023

industrial regions NPF and to understand the atmospheric organic-sulfur cycle more comprehensively.

Acknowledgments

This work was supported by the National Natural Science Foundation of China (No: 22203052; 22073059; 22006158); the Natural Science Foundation of Shaanxi Province (NO: 2022JM-060); the Key Cultivation Project of Shaanxi University of Technology (No: SLG2101); The Special Scientific Research Project of Hanzhong City-Shaanxi University of Technology Co-construction State Key Laboratory (SXJ-2106); The authors thank Prof. Qingzhu Zhang and Fei Xu from Shandong University for their sincere assistance in calculating the air-water interface reaction.

Declaration of competing interest

The authors declare that they have no known competing financial interests or personal relationships that could have appeared to influence the work reported in this paper.

Reference

Abedi, M., and Farrokhpour, H.: Acidity constants of some sulfur oxoacids in aqueous solution using CCSD and MP2 methods, Dalton Trans., 42, 5566-5572, 10.1039/C3DT33056G, 2013.

Akhmatskaya, E., Apps, C., Hillier, I., Masters, A., Palmer, I., Watt, N., Vincent, M., and Whitehead, J.: Hydrolysis of SO_3 and $ClONO_2$ in water clusters A combined experimental and theoretical study, J. Am. Chem. Soc., 93, 2775-2779, 1997.

Anglada, J. M., Hoffman, G. J., Slipchenko, L. V., M. Costa, M., Ruiz-Lopez, M. F., and Francisco, J. S.: Atmospheric significance of water clusters and ozone-water complexes, J. Phys. Chem. A, 117, 10381-10396, 2013.

Bandyopadhyay, B., Kumar, P., and Biswas, P.: Ammonia Catalyzed Formation of Sulfuric Acid in Troposphere: The Curious Case of a Base Promoting Acid Rain, J. Phys. Chem. A, 121, 3101-3108, 10.1021/acs.jpca.7b01172, 2017.

Becke, A. D.: Density-functional exchange-energy approximation with correct asymptotic behavior, Phys. Rev. A, 38, 3098-3100, 1988.

Bork, N., Elm, J., Olenius, T., and Vehkamäki, H.: Methane sulfonic acid-enhanced formation of molecular clusters of sulfuric acid and dimethyl amine, Atmos. Chem. Phys., 14, 12023-12030, 2014.

Calvert, J. G., Lazrus, A., Kok, G. L., Heikes, B. G., Walega, J. G., Lind, J., and Cantrell, C. A.: Chemical mechanisms of acid generation in the troposphere, Nature, 317, 27-35, 1985.

Cao, Y., Zhou, H., Jiang, W., Chen, C. W., and Pan, W. P.: Studies of the fate of sulfur trioxide in coal-fired utility boilers based on modified selected condensation methods, Environ. Sci. Technol., 44, 3429-3434, 2010.

Chen, L., and Bhattacharya, S.: Sulfur emission from Victorian brown coal under pyrolysis, oxy-fuel combustion and gasification conditions, Environ. Sci. Technol., 47, 1729-1734, 2013.

https://doi.org/10.5194/egusphere-2023-2009
Preprint. Discussion started: 13 October 2023

Chen, T., and Plummer, P. L.: Ab initio MO investigation of the gas-phase reaction sulfur trioxide + water. fwdarw. sulfuric acid, J. Phys. Chem. A, 89, 3689-3693, 1985.

Chen, X., Tao, C., Zhong, L., Gao, Y., Yao, W., and Li, S.: Theoretical study on the atmospheric reaction of SO_2 with the HO_2 and $HO_2{\cdot}H_2O$ complex formation HSO_4 and H_2SO_3, Chem. Phys. Lett., 608, 272-276, 2014.

Elm, J., Bilde, M., and Mikkelsen, K. V.: Influence of nucleation precursors on the reaction kinetics of methanol with the OH radical, J. Phys. Chem. A, 117, 6695-6701, 2013.

Elm, J., and Kristensen, K.: Basis set convergence of the binding energies of strongly hydrogen-bonded atmospheric clusters, Phys. Chem. Chem. Phys., 19, 1122-1133, 2017.

England, G. C., Zielinska, B., Loos, K., Crane, I., and Ritter, K.: Characterizing PM2. 5 emission profiles for stationary sources: comparison of traditional and dilution sampling techniques, Fuel Process. Technol., 65, 177-188, 2000.

Finlayson-Pitts, B. J., and Pitts Jr, J. N.: Atmospheric chemistry. Fundamentals and experimental techniques, John Wiley and Sons: New York, 1986.

Frisch, M. J., Head-Gordon, M., and Pople, J. A.: Semi-direct algorithms for the MP2 energy and gradient, Chem. Phys. Lett., 166, 281-289, https://doi.org/10.1016/0009-2614(90)80030-H, 1990.

Frisch, M. J., Trucks, G. W., Schlegel, H. B., Scuseria, G. E., Robb, M. A., Cheeseman, J. R., Scalmani, G., Barone, V., Mennucci, B., Petersson, G. A., Nakatsuji, H., Caricato, M., Li, X., Hratchian, H. P., Izmaylov, A. F., Bloino, J., Zheng, G., Sonnenberg, J. L., Hada, M., Ehara, M., Toyota, K., Fukuda, R., Hasegawa, J., Ishida, M., Nakajima, T., Honda, Y., Kitao, O., Nakai, H., Vreven, T., Montgomery, J. A., Jr., Peralta, J. E., Ogliaro, F., Bearpark, M., Heyd, J. J., Brothers, E., Kudin, K. N., Staroverov, V. N., Kobayashi, R., Normand, J., Raghavachari, K., Rendell, A., Burant, J. C., Iyengar, S. S., Tomasi, J., Cossi, M., Rega, N., Millam, J. M., Klene, M., Knox, J. E., Cross, J. B., Bakken, V., Adamo, C., Jaramillo, J., Gomperts, R., Stratmann, R. E., Yazyev, O., Austin, A. J., Cammi, R., Pomelli, C., Ochterski, J. W., Martin, R. L., Morokuma, K., Zakrzewski, V. G., Voth, G. A., Salvador, P., Dannenberg, J. J., Dapprich, S., Daniels, A. D., Farkas, Ö., Foresman, J. B., Ortiz, J. V., Cioslowski, J., and Fox, D. J: Gaussian09 Revision D. 01, Gaussian Inc. Wallingford CT, See also: URL: http://www. gaussian. com, 2009.

Gao, J., Wang, R., Zhang, T., Liu, F., and Wang, W.: Effect of methyl hydrogen sulfate on the formation of sulfuric acid-ammonia clusters: A theoretical study, J. Chin. Chem. Soc., 70, 689-698, https://doi.org/10.1002/jccs.202200148, 2023.

Glowacki, D. R., Liang, C.-H., Morley, C., Pilling, M. J., and Robertson, S. H.: MESMER: an open-source master equation solver for multi-energy well reactions, J. Phys. Chem. A, 116, 9545-9560, 2012.

Goedecker, S., Teter, M., and Hutter, J.: Separable dual-space Gaussian pseudopotentials, Phys. Rev. B, 54, 1703, 1996.

Gonzalez, J., Torrent-Sucarrat, M., and Anglada, J. M.: The reactions of SO_3 with HO_2 radical and $H_2O{\cdots}HO_2$ radical complex. Theoretical study on the atmospheric formation of HSO_5 and H_2SO_4, Phys. Chem. Chem. Phys., 12, 2116-2125, 2010.

Grimme, S., Antony, J., Ehrlich, S., and Krieg, H.: A consistent and accurate ab initio parametrization of density functional dispersion correction (DFT-D) for the 94 elements H-Pu, J. Chem. Phys., 132, 154104, 2010.

Hartwigsen, C., Goedecker, S., and Hutter, J.: Relativistic separable dual-space Gaussian pseudopotentials from H to Rn, Phys. Rev. B, 58, 3641-3662, 1998.

https://doi.org/10.5194/egusphere-2023-2009
Preprint. Discussion started: 13 October 2023

490 Haywood, J., and Boucher, O.: Estimates of the direct and indirect radiative forcing due to tropospheric
491 aerosols: A review, Rev. Geophys., 38, 513-543, 2000.
492 Hazra, M. K., and Sinha, A.: Formic acid catalyzed hydrolysis of SO_3 in the gas phase: A barrierless
493 mechanism for sulfuric acid production of potential atmospheric importance, J. Am. Chem. Soc.,
494 133, 17444-17453, 2011.
495 Hofmann, M., and Schleyer, P. v. R.: Acid rain: Ab initio investigation of the $H_2O{\bullet}SO_3$ complex and its
496 conversion to H_2SO_4, J. Am. Chem. Soc., 116, 4947-4952, 1994.
497 Horváth, G., Horváth, I., Almousa, S. A.-D., and Telek, M.: Numerical inverse Laplace transformation
498 using concentrated matrix exponential distributions, Perform. Evaluation, 137, 102067, 2020.
499 Huff, A. K., Mackenzie, R. B., Smith, C. J., and Leopold, K. R.: Facile Formation of Acetic Sulfuric
500 Anhydride: Microwave Spectrum, Internal Rotation, and Theoretical Calculations, J. Phys. Chem.
501 A, 121, 5659-5664, 10.1021/acs.jpca.7b05105, 2017.
502 Hutter, J., Iannuzzi, M., Schiffmann, F., and VandeVondele, J.: Wiley Interdiscip, Wiley Interdiscip. Rev.
503 Comput. Mol. Sci., 4, 15-25, 2014.
504 Kanno, N., Tonokura, K., and Koshi, M.: Equilibrium constant of the HO_2-H_2O complex formation and
505 kinetics of $HO_2 + HO_2$-H_2O: Implications for tropospheric chemistry, J. Geophys. Res.: Atmos., 111,
506 10.1029/2005jd006805, 2006.
507 Kikuchi, R.: Environmental management of sulfur trioxide emission: impact of SO_3 on human health,
508 Environ. Manage., 27, 837-844, 2001.
509 Kirkby, J., Curtius, J., Almeida, J., Dunne, E., Duplissy, J., Ehrhart, S., Franchin, A., Gagné, S., Ickes,
510 L., Kürten, A., Kupc, A., Metzger, A., Riccobono, F., Rondo, L., Schobesberger, S., Tsagkogeorgas,
511 G., Wimmer, D., Amorim, A., Bianchi, F., Breitenlechner, M., David, A., Dommen, J., Downard, A.,
512 Ehn, M., Flagan, R. C., Haider, S., Hansel, A., Hauser, D., Jud, W., Junninen, H., Kreissl, F., Kvashin,
513 A., Laaksonen, A., Lehtipalo, K., Lima, J., Lovejoy, E. R., Makhmutov, V., Mathot, S., Mikkilä, J.,
514 Minginette, P., Mogo, S., Nieminen, T., Onnela, A., Pereira, P., Petäjä, T., Schnitzhofer, R., Seinfeld,
515 J. H., Sipilä, M., Stozhkov, Y., Stratmann, F., Tomé, A., Vanhanen, J., Viisanen, Y., Vrtala, A.,
516 Wagner, P. E., Walther, H., Weingartner, E., Wex, H., Winkler, P. M., Carslaw, K. S., Worsnop, D.
517 R., Baltensperger, U., and Kulmala, M.: Role of sulphuric acid, ammonia and galactic cosmic rays
518 in atmospheric aerosol nucleation, Nature, 476, 429-433, 10.1038/nature10343, 2011.
519 Kulmala, M., Vehkamäki, H., Petäjä, T., Dal Maso, M., Lauri, A., Kerminen, V. M., Birmili, W., and
520 McMurry, P. H.: Formation and growth rates of ultrafine atmospheric particles: a review of
521 observations, J. Aerosol Sci., 35, 143-176, https://doi.org/10.1016/j.jaerosci.2003.10.003, 2004.
522 Kumar, M., Zhong, J., Francisco, J. S., and Zeng, X. C.: Criegee intermediate-hydrogen sulfide chemistry
523 at the air/water interface, Chem. Sci., 8, 5385-5391, 2017.
524 Kumar, M., Zhong, J., Zeng, X. C., and Francisco, J. S.: Reaction of Criegee Intermediate with Nitric
525 Acid at the Air-Water Interface, J. Am. Chem. Soc., 140, 4913-4921, 10.1021/jacs.8b01191, 2018.
526 Larson, L. J., Kuno, M., and Tao, F.-M.: Hydrolysis of sulfur trioxide to form sulfuric acid in small water
527 clusters, J. Chem. Phys., 112, 8830-8838, 2000.
528 Lee, C., Yang, W., and Parr, R. G.: Development of the Colle-Salvetti correlation-energy formula into a
529 functional of the electron density, Phys. Rev. B, 37, 785-789, 1988.
530 Li, H., Zhong, J., Vehkamäki, H., Kurtén, T., Wang, W., Ge, M., Zhang, S., Li, Z., Zhang, X., Francisco,
531 J. S., and Zeng, X. C.: Self-Catalytic Reaction of SO_3 and NH_3 To Produce Sulfamic Acid and Its
532 Implication to Atmospheric Particle Formation, J. Am. Chem. Soc., 140, 11020-11028,
533 10.1021/jacs.8b04928, 2018a.

https://doi.org/10.5194/egusphere-2023-2009
Preprint. Discussion started: 13 October 2023

534 Li, K., Song, X., Zhu, T., Wang, C., Sun, X., Ning, P., and Tang, L.: Mechanistic and kinetic study on the
535 catalytic hydrolysis of COS in small clusters of sulfuric acid, Environ. Pollut., 232, 615-623,
536 10.1016/j.envpol.2017.10.004, 2018b.
537 Li, L., Kumar, M., Zhu, C., Zhong, J., Francisco, J. S., and Zeng, X. C.: Near-barrierless ammonium
538 bisulfate formation via a loop-structure promoted proton-transfer mechanism on the surface of water,
539 J. Am. Chem. Soc., 138, 1816-1819, 2016.
540 Liu, J., Fang, S., Wang, Z., Yi, W., Tao, F. M., and Liu, J. Y.: Hydrolysis of sulfur dioxide in small clusters
541 of sulfuric acid: Mechanistic and kinetic study, Environ. Sci. Technol., 49, 13112-13120, 2015.
542 Liu, J., Liu, L., Rong, H., and Zhang, X.: The potential mechanism of atmospheric new particle formation
543 involving amino acids with multiple functional groups, Phys. Chem. Chem. Phys., 23, 10184-10195,
544 10.1039/D0CP06472F, 2021a.
545 Liu, L., Zhong, J., Vehkamäki, H., Kurtén, T., Du, L., Zhang, X., Francisco, J. S., and Zeng, X. C.:
546 Unexpected quenching effect on new particle formation from the atmospheric reaction of methanol
547 with SO_3, Proc. Natl. Acad. Sci. U.S.A., 116, 24966-24971, 2019.
548 Liu, L., Yu, F., Tu, K., Yang, Z., and Zhang, X.: Influence of atmospheric conditions on the role of
549 trifluoroacetic acid in atmospheric sulfuric acid-dimethylamine nucleation, Atmos. Chem. Phys., 21,
550 6221-6230, 10.5194/acp-21-6221-2021, 2021b.
551 Loerting, T., and Liedl, K. R.: Toward elimination of discrepancies between theory and experiment: The
552 rate constant of the atmospheric conversion of SO_3 to H_2SO_4, Proc. Natl. Acad. Sci. U. S. A., 97,
553 8874-8878, 2000.
554 Lohmann, U., and Feichter, J.: Global indirect aerosol effects: a review, J. Atmos. Chem. Phys., 5, 715-
555 737, 2005.
556 Long, B., Long, Z.-w., Wang, Y.-b., Tan, X.-f., Han, Y.-h., Long, C.-y., Qin, S.-j., and Zhang, W.-j.:
557 Formic Acid Catalyzed Gas-Phase Reaction of H_2O with SO_3 and the Reverse Reaction: A
558 Theoretical Study, ChemPhysChem, 13, 323-329, 10.1002/cphc.201100558, 2012.
559 Long, B., Chang, C. R., Long, Z. W., Wang, Y. B., Tan, X. F., and Zhang, W. J.: Nitric acid catalyzed
560 hydrolysis of SO_3 in the formation of sulfuric acid: A theoretical study, Chem. Phys. Lett., 581, 26-
561 29, 2013a.
562 Long, B., Tan, X.-F., Chang, C.-R., Zhao, W.-X., Long, Z.-W., Ren, D.-S., and Zhang, W.-J.: Theoretical
563 studies on gas-phase reactions of sulfuric acid catalyzed hydrolysis of formaldehyde and
564 formaldehyde with sulfuric acid and $H_2SO_4\cdots H_2O$ complex, J. Phys. Chem. A 117, 5106-5116,
565 2013b.
566 Lv, G., Sun, X., Zhang, C., and Li, M.: Understanding the catalytic role of oxalic acid in SO_3 hydration
567 to form H_2SO_4 in the atmosphere, Atmos. Chem. Phys., 19, 2833-2844, 2019.
568 Ma, X., Zhao, X., Ding, Z., Wang, W., Wei, Y., Xu, F., Zhang, Q., and Wang, W.: Determination of the
569 amine-catalyzed SO_3 hydrolysis mechanism in the gas phase and at the air-water interface,
570 Chemosphere, 252, 126292, 2020.
571 Mackenzie, R. B., Dewberry, C. T., and Leopold, K. R.: Gas phase observation and microwave
572 spectroscopic characterization of formic sulfuric anhydride, Science, 349, 58-61, 2015.
573 MacKerell, A. D., Bashford, D., Bellott, M., Dunbrack, R. L., Evanseck, J. D., Field, M. J., Fischer, S.,
574 Gao, J., Guo, H., Ha, S., Joseph-McCarthy, D., Kuchnir, L., Kuczera, K., Lau, F. T. K., Mattos, C.,
575 Michnick, S., Ngo, T., Nguyen, D. T., Prodhom, B., Reiher, W. E., Roux, B., Schlenkrich, M., Smith,
576 J. C., Stote, R., Straub, J., Watanabe, M., Wiórkiewicz-Kuczera, J., Yin, D., and Karplus, M.: All-

https://doi.org/10.5194/egusphere-2023-2009
Preprint. Discussion started: 13 October 2023

Atom Empirical Potential for Molecular Modeling and Dynamics Studies of Proteins, J. Phys. Chem. B, 102, 3586-3616, 10.1021/jp973084f, 1998.

McGrath, M. J., Olenius, T., Ortega, I. K., Loukonen, V., Paasonen, P., Kurtén, T., Kulmala, M., and Vehkamäki, H.: Atmospheric Cluster Dynamics Code: a flexible method for solution of the birth-death equations, Atmos. Chem. Phys., 12, 2345-2355, 10.5194/acp-12-2345-2012, 2012.

Miller, J. A., and Klippenstein, S. J.: Master equation methods in gas phase chemical kinetics, J. Phys. Chem. A, 110, 10528-10544, 2006.

Mitsui, Y., Imada, N., Kikkawa, H., and Katagawa, A.: Study of Hg and SO_3 behavior in flue gas of oxy-fuel combustion system, Int. J. Greenhouse Gas Control, 5, S143-S150, 2011.

Morokuma, K., and Muguruma, C.: Ab initio molecular orbital study of the mechanism of the gas phase reaction $SO_3 + H_2O$: Importance of the second water molecule, J. Am. Chem. Soc., 116, 10316-10317, 1994.

Myllys, N., Elm, J., Halonen, R., Kurten, T., and Vehkamaki, H.: Coupled cluster evaluation of the stability of atmospheric acid-base clusters with up to 10 molecules, J. Phys. Chem. A, 120, 621-630, 2016.

Otto, A. H., and Steudel, R.: Gas-Phase Structures and Acidities of the Sulfur Oxoacids $H_2S_nO_6$ (n = 2-4) and $H_2S_2O_7$, Eur. J. Inorg. Chem., 2001, 3047-3054, 2001.

Pérez-Ríos, J., Ragole, S., Wang, J., and Greene, C. H.: Comparison of classical and quantal calculations of helium three-body recombination, J. Chem. Phys., 140, 044307, 2014.

Pöschl, U.: Atmospheric aerosols: composition, transformation, climate and health effects, Angew. Chem., Int. Ed. Engl., 44, 7520-7540, 2005.

Pöschl, U., and Shiraiwa, M.: Multiphase chemistry at the atmosphere-biosphere interface influencing climate and public health in the anthropocene, Chem. Rev., 115, 4440-4475, 2015.

Renard, J. J., Calidonna, S. E., and Henley, M. V.: Fate of ammonia in the atmosphere-a review for applicability to hazardous releases, J. Hazard. Mater., 108, 29-60, 2004.

Riipinen, I., Sihto, S.-L., Kulmala, M., Arnold, F., Dal Maso, M., Birmili, W., Saarnio, K., Teinilä, K., Kerminen, V.-M., and Laaksonen, A.: Connections between atmospheric sulphuric acid and new particle formation during QUEST III-IV campaigns in Heidelberg and Hyytiälä, Atmos. Chem. Phys., 7, 1899-1914, 2007.

Rong, H., Liu, L., Liu, J., and Zhang, X.: Glyoxylic sulfuric anhydride from the gas-phase reaction between glyoxylic acid and SO_3: a potential nucleation precursor, J. Phys. Chem. A, 124, 3261-3268, 2020.

Shampine, L. F., and Reichelt, M. W.: The MATLAB ODE Suite, J. Sci. Comput., 18, 1-22, 10.1137/s1064827594276424, 1997.

Sihto, S.-L., Kulmala, M., Kerminen, V.-M., Dal Maso, M., Petäjä, T., Riipinen, I., Korhonen, H., Arnold, F., Janson, R., and Boy, M.: Atmospheric sulphuric acid and aerosol formation: implications from atmospheric measurements for nucleation and early growth mechanisms, Atmos. Chem. Phys., 6, 4079-4091, 2006.

Sipilä, M., Berndt, T., Petäjä, T., Brus, D., Vanhanen, J., Stratmann, F., Patokoski, J., Mauldin III, R. L., Hyvärinen, A.-P., and Lihavainen, H.: The role of sulfuric acid in atmospheric nucleation, Science, 327, 1243-1246, 2010.

Smith, C. J., Huff, A. K., Mackenzie, R. B., and Leopold, K. R.: Observation of Two Conformers of Acrylic Sulfuric Anhydride by Microwave Spectroscopy, J. Phys. Chem. A, 121, 9074-9080, 10.1021/acs.jpca.7b09833, 2017.

https://doi.org/10.5194/egusphere-2023-2009
Preprint. Discussion started: 13 October 2023

621 Starik, A., Savel'Ev, A., Titova, N., Loukhovitskaya, E., and Schumann, U.: Effect of aerosol precursors
622 from gas turbine engines on the volatile sulfate aerosols and ion clusters formation in aircraft plumes,
623 Phys. Chem. Chem. Phys., 6, 3426-3436, 2004.
624 Steudel, R.: Sulfuric acid from sulfur trioxide and water-a surprisingly complex reaction, Angew. Chem.
625 Int. Ed. Engl., 34, 1313-1315, 1995.
626 Stewart, J.: MOPAC2016 Stewart computational chemistry. Colorado Springs, CO: OpenMOPAC, in,
627 2016.
628 Stone, D., and Rowley, D. M.: Kinetics of the gas phase HO_2 self-reaction: Effects of temperature,
629 pressure, water and methanol vapours, Phys. Chem. Chem. Phys., 7, 2156-2163,
630 10.1039/B502673C, 2005.
631 Tan, X. F., Long, B., Ren, D. S., Zhang, W. J., Long, Z. W., and Mitchell, E.: Atmospheric chemistry of
632 CH_3CHO: the hydrolysis of CH_3CHO catalyzed by H_2SO_4, Phys. Chem.Chem.Phys., 20, 7701-7709,
633 2018.
634 Torrent-Sucarrat, M., Francisco, J. S., and Anglada, J. M.: Sulfuric acid as autocatalyst in the formation
635 of sulfuric acid, J. Am. Chem. Soc., 134, 20632-20644, 2012.
636 VandeVondele, J., and Hutter, J.: Gaussian basis sets for accurate calculations on molecular systems in
637 gas and condensed phases, J. Chem. Phys., 127, 114105, 2007.
638 Viegas, L. P., and Varandas, A. J.: Can water be a catalyst on the $HO_2 + H_2O + O_3$ reactive cluster?, Chem.
639 Phys., 399, 17-22, 2012.
640 Viegas, L. P., and Varandas, A. J.: The $HO_2 + (H_2O)_n + O_3$ reaction: an overview and recent developments,
641 Eur. Phys. J. D, 70, 1-9, 2016.
642 Wayne, R. P.: Chemistry of Atmospheres. An Introduction to the Chemistry of the Atmospheres of Earth,
643 the Planets, and Their Satellites, 3rd Oxford University Press, 10.1021/ja004780n, 2000.
644 Weber, R., McMurry, P., Eisele, F., and Tanner, D.: Measurement of expected nucleation precursor
645 species and 3-500-nm diameter particles at Mauna Loa observatory, Hawaii, J. Atmos. Sci., 52,
646 2242-2257, 1995.
647 Weber, R., Marti, J., McMurry, P., Eisele, F., Tanner, D., and Jefferson, A.: Measured atmospheric new
648 particle formation rates: Implications for nucleation mechanisms, Chem. Eng. Commun., 151, 53-
649 64, 1996.
650 Weber, R., Chen, G., Davis, D., Mauldin III, R., Tanner, D., Eisele, F., Clarke, A., Thornton, D., and
651 Bandy, A.: Measurements of enhanced H_2SO_4 and 3-4 nm particles near a frontal cloud during the
652 First Aerosol Characterization Experiment (ACE 1), J. Geophys. Res. Atmos., 106, 24107-24117,
653 2001.
654 Yang, Y., Liu, L., Wang, H., and Zhang, X.: Molecular-Scale Mechanism of Sequential Reaction of
655 Oxalic Acid with SO_3: Potential Participator in Atmospheric Aerosol Nucleation, J. Phys. Chem. A,
656 125, 4200-4208, 2021.
657 Yao, L., Garmash, O., Bianchi, F., Zheng, J., Yan, C., Kontkanen, J., Junninen, H., Mazon, S. B., Ehn,
658 M., Paasonen, P., Sipilä, M., Wang, M., Wang, X., Xiao, S., Chen, H., Lu, Y., Zhang, B., Wang, D.,
659 Fu, Q., Geng, F., Li, L., Wang, H., Qiao, L., Yang, X., Chen, J., Kerminen, V.-M., Petäjä, T., Worsnop,
660 D. R., Kulmala, M., and Wang, L.: Atmospheric new particle formation from sulfuric acid and
661 amines in a Chinese megacity, Science, 361, 278-281, doi:10.1126/science.aao4839, 2018.
662 Yao, L., Fan, X., Yan, C., Kurtén, T., Daellenbach, K. R., Li, C., Wang, Y., Guo, Y., Dada, L., Rissanen,
663 M. P., Cai, J., Tham, Y. J., Zha, Q., Zhang, S., Du, W., Yu, M., Zheng, F., Zhou, Y., Kontkanen, J.,
664 Chan, T., Shen, J., Kujansuu, J. T., Kangasluoma, J., Jiang, J., Wang, L., Worsnop, D. R., Petäjä, T.,

https://doi.org/10.5194/egusphere-2023-2009
Preprint. Discussion started: 13 October 2023

Kerminen, V. M., Liu, Y., Chu, B., He, H., Kulmala, M., and Bianchi, F.: Unprecedented Ambient Sulfur Trioxide (SO_3) Detection: Possible Formation Mechanism and Atmospheric Implications, Environ. Sci. Technol. Lett., 7, 809-818, 10.1021/acs.estlett.0c00615, 2020.

Zhang, H., Kupiainen-Määttä, O., Zhang, X., Molinero, V., Zhang, Y., and Li, Z.: The enhancement mechanism of glycolic acid on the formation of atmospheric sulfuric acid-ammonia molecular clusters, J. Chem. Phys., 146, 184308, 10.1063/1.4982929, 2017.

Zhang, H., Li, H., Liu, L., Zhang, Y., Zhang, X., and Li, Z.: The potential role of malonic acid in the atmospheric sulfuric acid-ammonia clusters formation, Chemosphere, 203, 26-33, 2018.

Zhang, J., and Dolg, M.: ABCluster: the artificial bee colony algorithm for cluster global optimization, Phys. Chem. Chem. Phys., 17, 24173-24181, 10.1039/C5CP04060D, 2015.

Zhang, J., and Dolg, M.: Global optimization of clusters of rigid molecules using the artificial bee colony algorithm, Phys. Chem. Chem. Phys., 18, 3003-3010, 10.1039/C5CP06313B, 2016.

Zhang, R., Khalizov, A., Wang, L., Hu, M., and Xu, W.: Nucleation and growth of nanoparticles in the atmosphere, Chem. Rev., 112, 1957-2011, 2012.

Zhang, R., Wang, G., Guo, S., Zamora, M. L., Ying, Q., Lin, Y., Wang, W., Hu, M., and Wang, Y.: Formation of urban fine particulate matter, Chem. Rev., 115, 3803-3855, 2015.

Zhang, R., Shen, J., Xie, H. B., Chen, J., and Elm, J.: The role of organic acids in new particle formation from methanesulfonic acid and methylamine, Atmos. Chem. Phys., 22, 2639-2650, 10.5194/acp-22-2639-2022, 2022.

Zhong, J., Kumar, M., Zhu, C. Q., Francisco, J. S., and Zeng, X. C.: Frontispiece: Surprising Stability of Larger Criegee Intermediates on Aqueous Interfaces, Angew. Chem. Int. Ed., 56, 7740-7744, 10.1002/anie.201782761, 2017.

Zhong, J., Kumar, M., Francisco, J. S., and Zeng, X. C.: Insight into chemistry on cloud/aerosol water surfaces, Acc. Chem. Res., 51, 1229-1237, 2018.

Zhong, J., Li, H., Kumar, M., Liu, J., Liu, L., Zhang, X., Zeng, X. C., and Francisco, J. S.: Mechanistic Insight into the Reaction of Organic Acids with SO_3 at the Air-Water Interface, Angew. Chem. Int. Ed., 131, 8439-8443, 2019.

Zhu, C., Kumar, M., Zhong, J., Li, L., Francisco, J. S., and Zeng, X. C.: New Mechanistic Pathways for Criegee-Water Chemistry at the Air/Water Interface, J. Am. Chem. Soc., 138, 11164-11169, 10.1021/jacs.6b04338, 2016.

Zhu, C., Kais, S., Zeng, X. C., Francisco, J. S., and Gladich, I.: Interfaces select specific stereochemical conformations: the isomerization of glyoxal at the liquid water interface, J. Am. Chem. Soc., 139, 27-30, 2017.

Zhuang, Y., and Pavlish, J. H.: Fate of hazardous air pollutants in oxygen-fired coal combustion with different flue gas recycling, Environ. Sci. Technol., 46, 4657-4665, 2012.

https://doi.org/10.5194/egusphere-2023-2009
Preprint. Discussion started: 13 October 2023

Table 1 The rate constant ($cm^3 \cdot molecule^{-1} \cdot s^{-1}$) for the $SO_3 + H_2SO_4$ reaction and the effective rate constant ($cm^3 \cdot molecule^{-1} \cdot s^{-1}$) for the $SO_3 + H_2SO_4$ reaction with H_2O (100%RH) within the temperature range of 280-320 K

T/(K)	280 K	290 K	298 K	300 K	310 K	320 K
k_{DSA}	5.52×10^{-12}	4.60×10^{-12}	3.95×10^{-12}	3.80×10^{-12}	3.13×10^{-12}	2.57×10^{-12}
$k'_{DSA\_WM\_o}$	2.12×10^{-13}	2.68×10^{-13}	2.88×10^{-13}	2.89×10^{-13}	2.89×10^{-13}	2.75×10^{-13}
$k'_{DSA\_WM\_s}$	1.03×10^{-11}	8.55×10^{-12}	7.42×10^{-12}	7.11×10^{-12}	5.79×10^{-12}	4.60×10^{-12}

k_{DSA} is the rate constant for the $SO_3 + H_2SO_4$ reaction; $k'_{DSA\_WM\_o}$ and $k'_{DSA\_WM\_s}$ are respectively the effective rate constants for H_2O-assisted $SO_3 + H_2SO_4$ reaction occurring through one-step and stepwise routes.

https://doi.org/10.5194/egusphere-2023-2009
Preprint. Discussion started: 13 October 2023

Table 2 Gibbs free energy (ΔG, kcal·mol^{-1}) for the formation of $S_2O_7^{2-}\cdots H_2SO_4$, $S_2O_7^{2-}\cdots HNO_3$, $S_2O_7^{2-}\cdots(COOH)_2$, $H_3O^+\cdots NH_3$, $H_3O^+\cdots H_2SO_4$, $HSO_4^-\cdots H_2SO_4$, $HSO_4^-\cdots(COOH)_2$, $HSO_4^-\cdots HNO_3$, $H_2SO_4\cdots NH_3$, $SO_7^{2-}\cdots H_2SO_4\cdots NH_3$, $HOOCCH_2COOH\cdots H_2SO_4\cdots NH_3$, $HOCCOOSO_3H\cdots H_2SO_4\cdots NH_3$, $CH_3OSO_3H\cdots H_2SO_4\cdots NH_3$ and $HOOCCH_2CH(NH_2)COOH\cdots H_2SO_4\cdots NH_3$ at 298 K

	$S_2O_7^{2-}\cdots H_2SO_4$	$S_2O_7^{2-}\cdots HNO_3$	$S_2O_7^{2-}\cdots(COOH)_2$	$H_3O^+\cdots NH_3$	$H_2SO_4\cdots NH_3$
ΔG	-46.3	-30.6	-39.9	-51.7 (-49.2)[a]	-8.9 (-8.9)[a]
	$H_3O^+\cdots H_2SO_4$	$HSO_4^-\cdots H_2SO_4$	$HSO_4^-\cdots(COOH)_2$	$HSO_4^-\cdots HNO_3$	$S_2O_7^{2-}$
ΔG	-27.5 (-27.0)[a]	-41.6	-33.6	-27.8	-40.1
	$HOOCCH_2COOH\cdots H_2SO_4\cdots NH_3$	$HOCCOOSO_3H\cdots H_2SO_4\cdots NH_3$	$CH_3OSO_3H\cdots H_2SO_4\cdots NH_3$	$HOOCCH_2CH(NH_2)COOH\cdots H_2SO_4\cdots NH_3$	$HOCH_2COOH\cdots H_2SO_4\cdots NH_3$
ΔG	-13.1 (-13.6)[b]	-20.4 (-22.5)[c]	-18.8 (-20.7)[d]	-13.2 (-14.0)[e]	-12.8 (-13.5)[f]

Energies are given in kcal·mol^{-1}, and calculated at the M06-2X/6-311++G(2*df*,2*pd*) theoretical level. References are as follows: [a] Zhong et al., 2019.; [b] Zhang et al., 2018.; [c] Rong et al., 2020.; [d] Gao et al., 2023.; [e] Liu et al., 2021a; [f] Zhang et al., 2017.

https://doi.org/10.5194/egusphere-2023-2009
Preprint. Discussion started: 13 October 2023

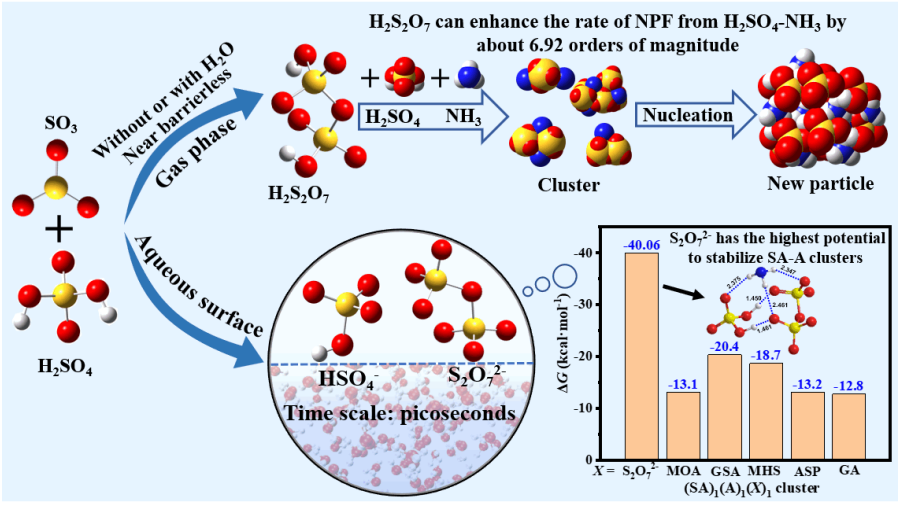

Graphic abstract

https://doi.org/10.5194/egusphere-2023-2009
Preprint. Discussion started: 13 October 2023

Figure Caption

Fig. 1 Schematic potential energy surface for the $SO_3 + H_2SO_4 \rightarrow H_2S_2O_7$ reaction; Distances is in angstrom at the M06-2X/6-311++G(2*df*,2*pd*) level, while the energy values correspond to the calculations at the CCSD(T)-F12/cc-pVDZ-F12//M06-2X/6-311++G(2*df*,2*pd*) level. The TS in the $SO_3 + H_2SO_4 \rightarrow H_2S_2O_7$ reaction without and with H_2O is denoted by "TS_{DSA}" and "TS_{DSA_WM}", respectively. The mark of a specific hydrogen bond complex depends on molecular formula and the connection sequence of each moiety.

Fig. 2 Top panel: Snapshot structures taken from the BOMD simulations, which illustrate H_2O-induced the formation of $S_2O_7^{2-}\cdots H_3O^+$ ion pair from the reaction of SO_3 with HSO_4^- at the air-water interface. Lower panel: time evolution of key bond distances (S-O1, O2-H1, and O3-H1) involved in the induced mechanism.

Fig. 3 Top panel: Snapshot structures taken from the BOMD simulations, which illustrate the hydration reaction mechanism of SO_3 mediated by HSO_4^- at the air water interface. Lower panel: time evolution of key bond distances (S-O1, O1-H2, O5-H2, O2-H1, O3-H4 and O4-H3) involved in the hydration mechanism.

Fig. 4 Top panel: Snapshot structures taken from the BOMD simulations, which illustrate the deprotonation of $H_2S_2O_7$ at the air water interface. Lower panel: time evolution of key bond distances (O1-HI, O1-H2, O3-H2 and H2-O4) involved in the hydration mechanism.

Fig. 5 The logarithms of the enhancement strength of DSA (lg*R*) as a function of [DSA] from 10^1 to 10^3 molecules cm^{-3} under different temperatures (218.15, 238.15, 258.15, 278.15 and 298.15 K) where [SA] = 10^7 molecules·cm^{-3} and [A] = 10^9 molecules·cm^{-3} (a); The logarithms of the enhancement strength of DSA (lg*R*) as a function of [A] from 10^7 to 10^{11} molecules cm^{-3} at T = 278.15 K and [DSA] = 10^3 molecules·cm^{-3} under different [SA] = 10^6-10^8 molecules·cm^{-3} (b).

Fig. 6 The main pathways of clusters growing out of the research system under the conditions where T = 278.15 K, [SA] = 10^7 molecules·cm^{-3}, [A] = 10^{11} molecules·cm^{-3}, and [DSA] = 10^3 molecules·cm^{-3} (A). The pure SA-A-based cluster pathway (a) and the DSA-containing pathway (b). The black and blue fluxes represent the pathways of the SA-A-based cluster and the SA-A-DSA-based cluster, respectively. The effects of temperature (B), [DSA] (C), and [SA] (D) on the relative contribution of the pure SA-A-based cluster pathway and the DSA-containing pathway to the flux out of the system. Others in (B), (C), and (D) indicate that the pathway contribution of the cluster growing out of the studied system is less than 5%.

https://doi.org/10.5194/egusphere-2023-2009
Preprint. Discussion started: 13 October 2023

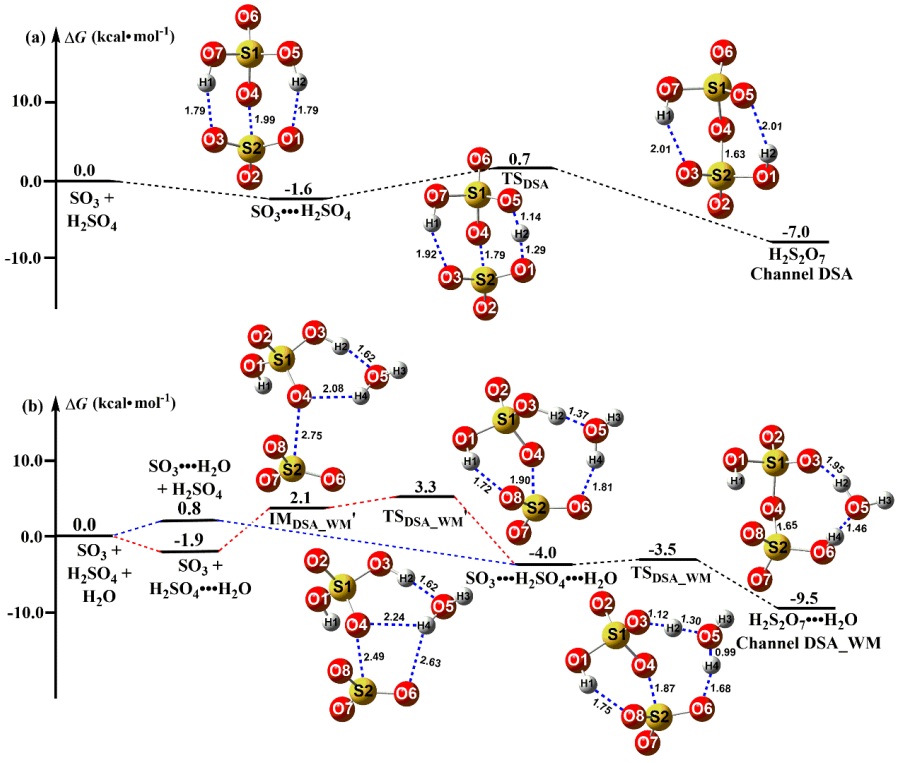

Fig. 1

https://doi.org/10.5194/egusphere-2023-2009
Preprint. Discussion started: 13 October 2023

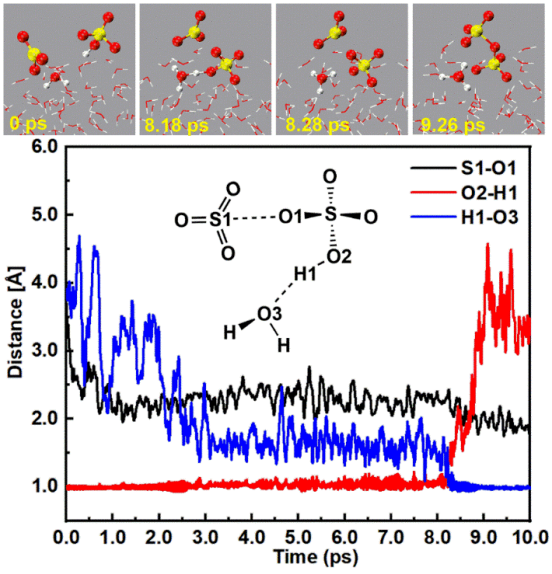

Fig. 2

https://doi.org/10.5194/egusphere-2023-2009
Preprint. Discussion started: 13 October 2023

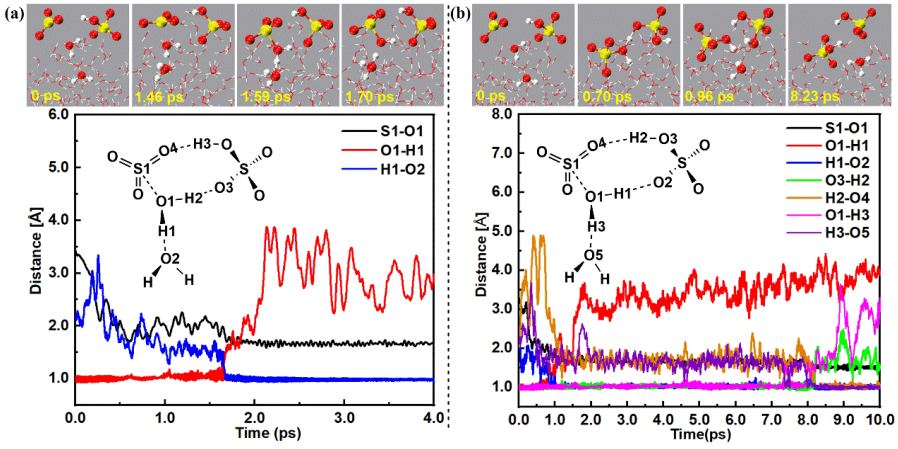

Fig. 3

https://doi.org/10.5194/egusphere-2023-2009
Preprint. Discussion started: 13 October 2023

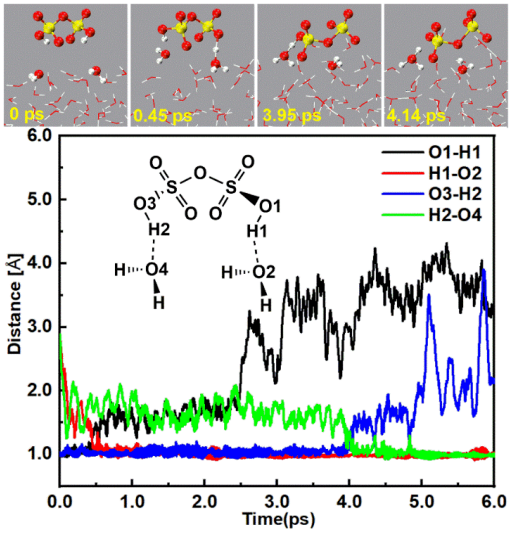

Fig. 4

https://doi.org/10.5194/egusphere-2023-2009
Preprint. Discussion started: 13 October 2023

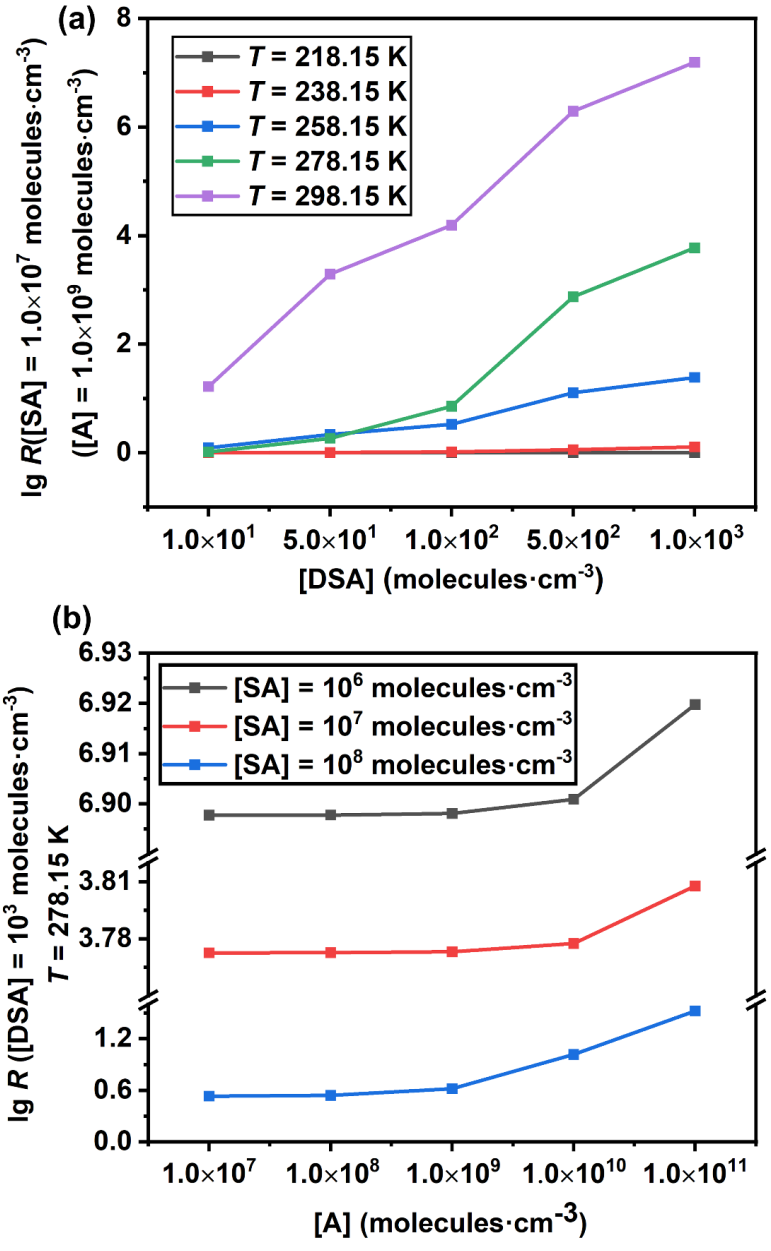

Fig. 5

https://doi.org/10.5194/egusphere-2023-2009
Preprint. Discussion started: 13 October 2023

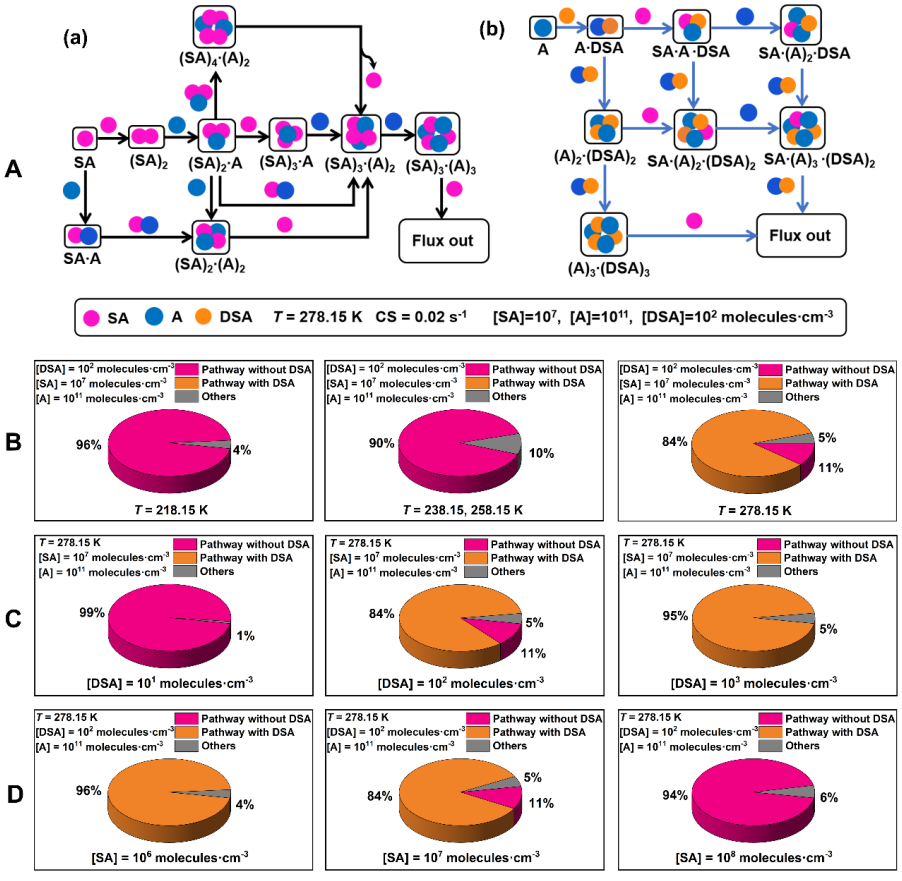

Fig. 6